

1 **Influence of Meteorology and interrelationship with greenhouse gases (CO₂**
2 **and CH₄) at a suburban site of India**

3 Sreenivas. G, Mahesh. P*, Subin Jose, Kanchana A. L., Rao P.V.N, Dadhwal. V.K

4 Atmospheric and Climate Sciences Group (ACSG),

5 Earth and Climate Science Area (ECSA),

6 National Remote Sensing Center (NRSC),

7 Indian Space Research Organization (ISRO),

8 Hyderabad, India-500037

9
10 *Corresponding author: Mahesh P

11 Mail-Id:mahi952@gmail.com

12

13

14

15

16

17

18

19

20

21

22

23

24 **Abstract**

25 Atmospheric greenhouse gases (GHGs), such as carbon dioxide (CO₂) and methane
26 (CH₄), are important climate forcing agents due to their significant impacts on the climate
27 system. The present study brings out first continuous measurements of atmospheric GHGs using
28 high precision LGR-GGA over Shadnagar, a suburban site of Central India during the period
29 2014. The annual mean CO₂ and CH₄ over the study region are found to be 394±2.92 ppm and
30 1.92±0.07 ppm ($\mu \pm 1\sigma$) respectively. CO₂ and CH₄ show a significant seasonal variation during
31 the study period with maximum (minimum) CO₂ observed during Pre-monsoon (Monsoon),
32 while CH₄ recorded maximum during post-monsoon and minimum in monsoon. Irrespective of
33 the seasons, consistent diurnal variations of these gases are observed. Influences of prevailing
34 meteorology (air temperature, wind speed, wind direction and relative humidity) on GHGs have
35 also been investigated. CO₂ and CH₄ show a strong positive correlation during winter, pre-
36 monsoon, monsoon, and post-monsoon with correlation coefficients (Rs) equal to 0.80, 0.80,
37 0.61, and 0.72 respectively; indicating common anthropogenic source for these gases. Analysis of
38 this study reveals the major sources for CO₂ are soil respiration and anthropogenic emissions
39 while vegetation act as a main sink. Whereas the major source and sink for CH₄ are vegetation
40 and presence of hydroxyl (OH) radicals.

41

42 Keywords: Carbon dioxide, Methane, OH radical.

43

44

45

46

47

48

49

50

51 **1. Introduction**

52 The Intergovernmental Panel on Climate Change (IPCC, 2013) reported that humankind is
53 causing global warming through the emission of greenhouse gases (GHGs), particularly carbon
54 dioxide (CO₂) and methane (CH₄). CO₂ and CH₄ concentrations have increased by 40% and 150
55 % respectively since pre-industrial times, mainly from fossil fuel emissions and secondarily from
56 net land use change emissions (IPCC, 2013; Huang et al., 2015). CO₂ measurements at
57 MaunaLoa, Hawaii (Monastersky, 2013) have exceeded the 400 ppm mark several times in May
58 2013. CH₄ is also receiving increasing attention due to high uncertainty in its sources and sinks
59 (Keppler et al., 2006; Miller et al., 2007; Frankenberg et al., 2008). Stefanie Kirschke et al.,
60 (2013) reported that in India, agriculture and waste constitute the single largest regional source
61 of CH₄. Although many sources and sinks have been identified for CH₄, their relative
62 contribution to atmospheric CH₄ is still uncertain (A. Garg et al., 2001; StefanieKirschke et al.,
63 2013). In India, electric power generation contributes to half of India's total CO₂ equivalent
64 emissions (A. Garg et al., 2001).

65 Arid and semi-arid areas comprise about 30% of the Earth's land surface. Climate change
66 and climate variability will likely have a significant impact on these regions (Huang et al., 2008;
67 Huang et al., 2015). The variability of environmental factors may result in significant effects on
68 regional climate and global climate (Wang et al., 2010), especially the radiative forcing; via the
69 biogeochemical pathways affecting the terrestrial carbon cycle. Global climate change has
70 serious impact on humans and ecosystems. Due to this, many factors have been identified that
71 may reflect or cause variations in environmental change (Pielke et al., 2002). Out of these, the
72 Normalized Difference Vegetation Index (NDVI) has become one of the most widely used
73 indices to represent the biosphere influence on global change (Liu et al., 2011). Greenhouse and
74 other trace gases have great importance in atmospheric chemistry and for radiation budget of the
75 atmosphere-biosphere system (Crutzen et al., 1991). Hydroxyl radicals (OH) are very reactive
76 oxidizing agents, which are responsible for the oxidation of almost all gases that are emitted by
77 natural and anthropogenic activities in the atmosphere. Atmospheric CO₂ measurements are very
78 important for understanding the carbon cycle because CO₂ mixing ratios in the atmosphere are
79 strongly affected by photosynthesis, respiration, oxidation of organic matter, biomass and fossil
80 fuel burning, and air-sea exchange process (Machida et al., 2003).

81 The present study brings out first continuous measurements of atmospheric GHGs using high
82 precision LGR-GGA over Shadnagar, a suburban site of Central India during the period 2014. In
83 addition to GHGs observations, we have also made use of an automatic weather station (AWS)
84 data along with model/satellite retrieved observation during the study period. Details about study
85 area and data sets are described in the following sections.

86 **2. Study Area**

87 Shadnagar is situated in Mahabubnagar district of newly formed Indian state of
88 Telangana. It is a suburban location situated ~70 km away from urban site of Hyderabad
89 (Northern side) with a population of ~0.16 million (Patil et al., 2013). A schematic map of study
90 area is shown in Fig. 1a. Major sources of pollutants over Shadnagar can be from small and
91 medium scale industries, biomass burning and bio-fuel as well as from domestic cooking. In the
92 present study sampling of GHGs and related meteorological parameters are carried out in the
93 premises of National Remote Sensing Center (NRSC), Shadnagar Campus (17°02'N, 78°11'E).
94 Sampling site is near (aerial distance ~ 2.25 km) to National highway 7 (NH7) and a railway
95 track (non-electrified) is in the East (E) direction.

96 Mean monthly variations of temperature (°C) and relative humidity (RH %) observed at
97 Shadnagar during 2014 are shown in Figure 1e and 1d respectively. The Indian Meteorological
98 Department (IMD) defined monsoon as June-July-August-September (JJAS), post-monsoon
99 (October-November-December-OND), winter (January-February-JF) and pre-monsoon (March-
100 April-May-MAM) in India. Temperature over Shadnagar varies from ~20°C to ~29°C. Relative
101 humidity (RH) in Shadnagar reached a maximum of ~82 % in monsoon from a minimum of ~48
102 % recorded during pre-monsoon. Surface wind speed (Fig. 1c) varies between 1.3 to 1.6 m s⁻¹
103 with a maximum observed during monsoon and minimum in pre-monsoon. The air mass
104 advecting (Fig. 1b) towards study site is either easterly or westerly. The easterly wind prevails
105 during winter and gradually shifts to south-westerlies in pre-monsoon, and dominates during
106 monsoon.

107 **3. Data set and Methodology**

108 Details about the instrument and data utilized are discussed in this section. The availability
109 and frequency of the observations all data used in present study are tabulated in Table 1.

110

111 **3.1 In-situ observations**

112 3.1.1 Greenhouse Gas Analyser (GGA)

113 The Los Gatos Research's - Greenhouse Gas Analyser (model: LGR-GGA-24EP) is an
114 advanced instrument capable of simultaneous measurements of CO₂, CH₄ and H₂O. This
115 instrument is well known for high precision and accuracy which are crucial towards
116 understanding background concentrations of atmospheric GHGs, with specifications meeting
117 WMO standards of measurement (Berman et al., 2012; Shea et al., 2013; Mahesh et al., 2015). It
118 is based on enhanced Off-Axis Integrated Cavity Output Spectroscopy (OA-ICOS) technology
119 (Paul et al. 2001, Baer et al., 2002), which utilizes true wavelength scanning to record fully
120 resolved absorption line shapes. Considering the nature of the site, flow rate is fixed to be 7
121 liters per minute (lpm). Ambient air entering the GGA is analysed using two near infrared (NIR)
122 distributed feedback tunable diode lasers (TDL), one for a CO₂ absorption line near 1.60 μm ($\nu_0 =$
123 6250 cm^{-1}) and the other to probe CH₄ and H₂O absorption lines near 1.65 μm ($\nu_0 = 6060.60 \text{ cm}^{-1}$).
124 The concentration of the gases is determined by the absorption of their respective
125 characteristic absorption lines with a high sampling time of 1sec. A detailed explanation
126 regarding the configuration, working and calibration procedure performed for GGA in NRSC
127 can be found elsewhere in Mahesh et al., (2015). In the present study we used GGA retrieve CO₂
128 and CH₄ data. High resolution data sets are diurnally averaged and used in further analysis. Due
129 to failure of internal central processing unit (CPU) of the analyzer, data are not recorded from
130 pre-monsoon month of 1st May to 18th June during the study period.

131 3.1.2 O₃ and NO_x analyzer

132 Surface concentrations of O₃ and NO_x have been measured continuously using on-line
133 analyzers (Model No.s: 49i and 42i for O₃ and NO_x respectively), procured from Thermo
134 Scientific, USA since July 2014. The trace gases (O₃ and NO_x) sampling inlet is installed on the
135 top of a 2 m mast fixed on the roof of an 8 m high building, and ambient air flow is supplied to
136 the instruments. The inlet prevents the ingress of rain water, and is equipped with 0.5 μm filter to
137 prevent accumulation of dust within the instrument. The ozone analyzer is based on Beer-
138 Lambert-Baugher law which relates absorption of light to the concentration of species as its
139 operating principle and has an in-built calibration unit for conducting periodical span and zero
140 checks. The NO_x analyzer utilizes a molybdenum converter to convert NO₂ into NO and

141 estimates the NO_x concentration by the intensity of light emitted during the chemiluminescent
142 reaction of NO with O₃ present in the ambient air. The analyzer is integrated with zero and span
143 calibrations which are performed twice monthly.

144 Simultaneous observations of meteorological parameters are obtained from an automatic
145 weather station (AWS) installed in NRSC, Shadnagar campus as a part of Calibration and
146 Validation (CAL/VAL) project in March 2012 is equipped with nine sensors to measure fifteen
147 weather parameters. Weather parameters measured are at surface level and height of the AWS
148 mast is ~10 meters.

149 **3.2 Satellite and Model observations**

150 **3.2.1 MODIS**

151 Moderate-resolution Imaging Spectrometer (MODIS) is launched in December 1999 on the
152 polar-orbiting NASA-EOS Terra platform (Salomonson et al. 1989; King et al. 1992). It has 36
153 spectral channels and acquires data in 3 spatial resolutions of 250 m, 500 m, and 1 km (channels
154 8–36), covering the visible, near-infrared, shortwave infrared, and thermal-infrared bands. In the
155 present study we used monthly Normalised Difference Vegetation Index (NDVI) data obtained
156 from Terra/MODIS at 5 km spatial resolution. The NDVI value is defined as following ratio of
157 albedos (α) at different wavelengths:

$$158 \quad \text{NDVI} = \frac{\alpha_{0.86\mu\text{m}} + \alpha_{0.67\mu\text{m}}}{\alpha_{0.86\mu\text{m}} - \alpha_{0.67\mu\text{m}}} \quad (1)$$

159 NDVI values can range from -1.0 to 1.0 but typical ranges are from 0.1 to 0.7, with higher values
160 associated with greater density and greenness of plant canopies. More details of the processing
161 methods used in generating the data set can be found in James and Kalluri (1994).

162 **3.2.2 COSMIS-RO**

163 COSMIC (Constellation Observation System for Meteorology, Ionosphere and Climate) is a
164 GPS (Global Positioning System) radio occultation (RO) observation system (Wang et al., 2013).
165 It consists of six identical microsatellites, and was launched successfully on 14 April 2006. GPS
166 radio occultation observation has the advantage of near-global coverage, all-weather capability,
167 high vertical resolution, high accuracy and self-calibration (Yunck et al., 2000). Geophysical
168 parameters (such as, temperature and humidity profiles) have been simultaneously obtained from
169 refractivity data using one-dimensional variational (1DVAR) analysis. Further COSMIC-RO

170 profiles are used to estimate planetary boundary layer height (BLH). BLH is defined to be the
171 height at which the vertical gradient of the refractivity or water vapor partial pressure is
172 minimum (Ao et al., 2012), explained detail methodology for calculating the BLH from
173 refractivity (N). The planetary boundary layer (PBL) is part of the atmosphere closest to the
174 Earth's surface where turbulent processes often dominate the vertical redistribution of sensible
175 heat, moisture, momentum, and aerosols/pollution (AO et al., 2012).

176 3.2.3 Hysplit model

177 The general air mass pathway reaching over Shadnagar is analysed using HYSPLIT model
178 (Draxler and Rolph, 2003) [<http://ww.arl.noaa.gov/ready/hysplit4.html>]. We computed 5 day
179 isentropic model backward air mass trajectory for all study days with each trajectory starting at
180 00:60 UTC and reaching study site, (Shadnagar) at different altitudes(1 km,2 km,3km and 4 km).
181 Even though the trajectory analysis have inherent uncertainties (Stohl, 1998), they are quite
182 useful in determining long range circulation.

183 4. Results and Discussion

184

185 4.1 Seasonal variations of CO₂ and CH₄

186 Temporal variations of CO₂ and CH₄ during the study period are shown in Figure 2a and 2b.
187 The circles indicate the daily mean, while triangular markers represent weakly averages and
188 monthly mean by square markers. Annual mean of CO₂ over study region is found to be
189 394±2.92 (mean (μ) ± standard deviation (1σ)) ppm with an observed minimum in monsoon and
190 maximum in pre-monsoon. Seasonal mean values of CO₂ observed during different seasons are
191 393±5.60, 398±7.60, 392±7.0, and 393±7.0 ppm in winter, pre-monsoon, monsoon, and post-
192 monsoon respectively. Minimum CO₂ during winter (dry season) can be due to respiratory loss
193 of carbon (Gilmanov et al., 2004; Aurela et al. 2004) as decreased temperature and solar
194 radiation during this period inhibit increases in local CO₂ assimilation (Thum et al., 2009). A
195 steady increase in CO₂ concentration is observed as season changes from winter to pre-monsoon
196 months. Enhancement in pre-monsoon is due to higher temperature and solar radiation
197 prevailing during these months which stimulate the assimilation of CO₂ in the daytime and
198 respiration in the night (Fang et al., 2014). The enhanced soil respiration during these months
199 also compliments the increase in CO₂ concentration during this period. In addition to these

200 natural causes, biomass burning over Indian region can also have a significant effect on pre-
201 monsoon CO₂ concentration. More detailed explanation of biomass burning influence on pre-
202 monsoon GHGs concentration over study area is discussed in section 4.2. Surface CO₂
203 concentration recorded a minimum during monsoon months can be mainly because of enhanced
204 photosynthesis processes with the availability of greater soil moisture. A decrease in CO₂
205 concentration is also observed as the monsoon progress. The decreases in temperature (due to
206 cloudy and overcast conditions prevailing during these months) reduce leaf and soil respiration
207 which contributes to the enhancement of carbon uptake (Patil et al., 2013; Jing et al., 2010).
208 Further increase during post-monsoon CO₂ is associated with high ecosystem productivity
209 (Sharma et al., 2014) also an enhancement in soil microbial activity (Stefanie Kirschke et al.,
210 2013).

211 CH₄ concentration in the troposphere is principally determined by a balance between surface
212 emission and destruction by hydroxyl radicals (OH). The major sources for CH₄ in the Indian
213 region are rice, paddies, wetlands and ruminants (Schneising et al., 2009). Annual CH₄
214 concentration over study area is observed to be 1.92 ± 0.07 ppm, with a maximum (2.02 ± 0.01
215 ppm) observed in post-monsoon and minimum (1.85 ± 0.03 ppm) in monsoon. Seasonal mean
216 (average) values of CH₄ observed during different seasons are 1.93 ± 0.05 , 1.89 ± 0.05 , 1.85 ± 0.03 ,
217 and 2.02 ± 7 ppm with respectively winter, pre-monsoon, monsoon, and post-monsoon. The
218 highest concentration appears during post-monsoon and may be associated with the Kharif
219 season (Goroshiet al., 2011). Hayashida et al. (2013) reported that the seasonality of CH₄
220 concentration over monsoon Asia is characterized by higher values in the wet season and lower
221 values in the dry season; possibly because of the effects of strong emissions from rice paddies
222 and wetlands during the wet season. Low mixing ratios of CH₄ observed during monsoon season
223 were mainly due to the reduction in atmospheric hydrocarbons because of the reduced
224 photochemical reactions and the substantial reduction in solar intensity (Abhishek Gaur et al
225 2014). The rate of change of CH₄ was found to be high during post-monsoon. Both biological and
226 physical processes control the exchange of CH₄ between rice paddy fields and the atmosphere
227 (Nishanth et al., 2014; Goroshiet al., 2011). Due to this, enhanced CH₄ observed during post-
228 monsoon at present study area..

229 ***4.2 Influence of vegetation on GHGs.***

230 In India cropping season is classified into (i) Kharif and (ii) Rabi based on the onset of
231 monsoon. The Kharif season is from July to October during the south-west (SW) monsoon and
232 Rabi season is from October to March (Koshal Avadhesh, 2013). NDVI being one of the
233 indicators of vegetation change, monthly variations of CO₂ and CH₄ against NDVI is studied to
234 understand the impact of land use land cover on mixing ratios of CO₂ and CH₄. Monthly mean
235 changes in NDVI, CO₂ and CH₄ are shown in Figure 2c and 2d. Monthly mean of GHGs
236 represented in this analysis is calculated from daily mean in day time (10-16 LT). Analysis of the
237 figure reveals that an inverse relationship exists between NDVI and CO₂; while a positive
238 relation is observed w.r.t CH₄. Generally over this part of the country vegetation starts during
239 the month of June with the onset of SW monsoon and as vegetation increases a decrease in CO₂
240 concentration is observed, due to enhancement in photosynthesis. Further a decline in NDVI is
241 observed as the season advances from post monsoon to winter and then to pre-monsoon, and it is
242 associated with an increase in CO₂ concentration. Similarly, the main source for CH₄ emissions
243 are soil microbial (Stefanie Kirschke et al., 2013) activity which are more active during monsoon
244 and post monsoon seasons.

245 Biomass burning (forest fire and crop residue burning) is one of the major sources of gaseous
246 pollutants such as carbon monoxide (CO₂), methane (CH₄), nitrous oxides (NO_x) and
247 hydrocarbons in the troposphere (Crutzen et al., 1990, 1985; Sharma et al., 2010). In one of the
248 recent studies Jose et al, (2015a) analysed the atmospheric impact due to biomass mass burning
249 over Hyderabad. In order to study the role of biomass burning on GHGs a case study is
250 discussed. Figure 3c shows the spatial distribution of MODIS derived fire counts over Indian
251 region during 14-21 April 2014 with air mass trajectories ending over study area over layed on it
252 at different altitudes viz. 1000 m, 2000 m and 4000 m respectively. Analysis of the figure shows
253 a number of potential fire locations on the north-western and south-eastern side of study location
254 and trajectories indicate its possible transport to study area. Daily mean variation of GHGs
255 during the month of April 2014 (Figure 3b) indicates an enhancement in GHGs during the same
256 period (14-21 April 2014). Analysis reveals that CO₂ and CH₄ have increased by ~2% and
257 ~0.06% respectively during event days with respect to monthly mean. This analysis reveals that
258 long range / regional transported biomass burning have a role in enhancement of GHGs over
259 study site. Further to understand the seasonal variation of biomass burning contribution to GHGs
260 we analysed long term (2003-2013) Fire Energetics and Emissions Research version 1.0 (FEER

261 v1) data over study area. Emission coefficient (C_e) products during biomass burning is developed
262 from coincident measurements of fire radiative power (FRP) and AOD from MODIS Aqua and
263 Terra satellites (Ichoku and Ellison, 2014). Figure 3a shows seasonal variation of CO_2 emission
264 due to biomass burning over the study site. Enhancement in CO_2 emission is seen during pre-
265 monsoon months; which also supports earlier observation (Figure 2a). This analysis reveals that
266 biomass burning has a role in pre-monsoon enhancement of CO_2 over study site. For a qualitative
267 analysis of this long range transport, we have analysed air mass trajectories ending over study
268 site during different seasons.

269 **4.3 Correlation between CO_2 and CH_4**

270 A correlation study is carried out between hourly averaged CO_2 and CH_4 during all season
271 for the entire study period. The statistical analysis for different seasons is shown in Table 2. Fang
272 et al., (2015) suggest the correlation coefficients (R_s) value higher than 0.50 indicates a similar
273 source mechanism of CO_2 and CH_4 . Also a positive correlation dominance of anthropogenic
274 emission on carbon cycle. Our study also reveals a strong positive correlation observed between
275 CO_2 and CH_4 during winter, pre-monsoon, monsoon, and post-monsoon with R equal to 0.80,
276 0.80, 0.61, and 0.72 respectively. Seasonal regression coefficients (slope) and their uncertainties
277 (Ψ_{slope} , Ψ_{y-int}) are computed using Taylor (1997) which showed maximum during winter, pre-
278 monsoon, and minimum in a monsoon that figure out the hourly stability of the mixing ratios
279 between CO_2 and CH_4 . This can be due to relatively simple source/sink process of CO_2 in
280 comparison with CH_4 . Figure 4 shows the seasonal variation of $\Delta CH_4/\Delta CO_2$. Dilution effects
281 during transport of CH_4 and CO_2 can be minimized to some extent by dividing the increase of
282 CH_4 over time by the respective increase in CO_2 (Worthy et al., 2009). In this study, background
283 concentrations of respective GHGs are determined as mean values of the 1.25 percentile of data
284 for monsoon, post-monsoon, pre-monsoon and winter (Pan et al., 2011; Worthy et al., 2009).
285 Annual $\Delta CH_4/\Delta CO_2$ over the study region during the study period is found to be 7.1 (ppb/ppm).
286 This low value clearly indicates the dominance of CO_2 over the study region. The reported
287 $\Delta CH_4/\Delta CO_2$ values from some of the rural sites viz Canadian Arctic and Hateruma Island
288 (China) are of the order 12.2 and ~ 10 ppb/ppm respectively (Worthy et al., 2009; Tohjima et al.,
289 2014). Average $\Delta CH_4/\Delta CO_2$ ratio during winter, pre-monsoon, monsoon and post-monsoon are
290 9.40, 6.40, 4.40, and 8.20 ppb respectively. Monthly average, of $\Delta CH_4/\Delta CO_2$, is relatively high

291 from late post-monsoon to winter, when the biotic activity is relatively dormant (Tohjima et al.,
292 2014). During pre-monsoon decrease in $\Delta\text{CH}_4/\Delta\text{CO}_2$ ratio indicates the enhancement of CO_2
293 relative to that of CH_4 .

294 ***4.4 Diurnal variations of CO_2 and CH_4***

295 Figure 5a to 5d shows the seasonally averaged diurnal cycle of CO_2 and CH_4 over Shadnagar
296 during study period. The vertically bar represents the standard deviation from respective mean.
297 Irrespective of seasonal variation GHGs showed a similar diurnal variation, with maximum
298 mixing ratios observed during early morning (06:00 hrs) as well as early night hours (20:00 hrs)
299 and minimum during afternoon hours. However the difference observed in the maximum diurnal
300 amplitudes can be attributed to seasonal changes. The observed diurnal cycle of GHGs is closely
301 associated with diurnal variation of planetary boundary layer height (PBLH). For better
302 understanding of the diurnal behavior of CO_2/CH_4 , we used European Centre for Medium-range
303 Weather Forecasting (ECMWF) Interim Reanalysis (ERA) PBL data set which gives the data for
304 every three hours viz. 00:00, 03:00, 06:00, 09:00, 12:00, 15:00, 18:00, and 21:00 UTC with a
305 resolution of $0.25^\circ \times 0.25^\circ$ (<http://data-portal.ecmwf.int>). Figure 5a to 5d portrays the diurnal
306 evolution of CO_2/CH_4 during different season along with the evolution of Boundary Layer
307 Height (m) on secondary y axis. The morning peak arises due to combined influence of
308 fumigation effect, (Stull 1988) and morning build-up of local anthropogenic activities (household
309 and vehicular transport). Low value of GHGs as the day progress can be attributed to increased
310 photosynthetic activity during day time and destruction of stable boundary layer and residual
311 layer due convective activity. In the evening hours, surface inversion begins and form a shallow
312 stable boundary layer causing the enhancement in GHGs concentration near the surface. Similar
313 trend in diurnal variation of GHGs is reported from other parts of the country (Patil et al., 2013;
314 Mahesh et al., 2014; Sharma et al., 2014; Nishanth et al., 2014).

315 ***4.5 Influence of prevailing meteorology***

316 Redistribution (both horizontal and vertical) of GHGs also plays a role in their seasonal
317 variation, as it controls transport and diffusion of pollutants from one place to another (Hassan
318 2015). A good inverse correlation between wind speed and GHGs suggest the proximity of
319 sources near measurement site, while a not so significant correlation suggests the influence of
320 regional transport (Ramachandran and Rajesh, 2007). Figure 6a and 6b shows scatter plot

321 between GHGs and wind speed during different seasons. Analysis of Figure 6 shows that there
322 exists an inverse correlation between daily mean wind speed and GHGs. Correlation coefficients
323 (Rs) between wind speed and CO₂ during pre-monsoon, monsoon, post-monsoon, and winter is
324 0.56, 0.32, 0.06, and 0.67 respectively. While for CH₄ it is found to be 0.28, 0.71, 0.21, and 0.60
325 respectively. Negative correlation indicates that the influence of local sources on GHGs,
326 however, poor correlation coefficients during different seasons suggest the role of regional/local
327 transport (Mahesh et al 2014). Also an understanding of prevailing wind direction and its
328 relationship with GHGs helps in determining their probable source regions. Table 3 shows the
329 monthly mean variation of CO₂ and CH₄ with respect to different wind direction. Enhancement
330 in CO₂ and CH₄ level over Shadnagar are observed to mainly come from NW and NE while the
331 lowest is from the S and SW. This can be associated to some extent with industrial emissions
332 located in western side of sampling site, and the influence of emission and transport from nearby
333 urban center on the NW side of the study site.

334 The influence of meteorological parameters (temperature and relative humidity) on trace
335 gases is also examined. Figure 7a and 7b (top panel corresponds to CO₂ and bottom panel
336 represents CH₄) show the scatter plot of temperature versus relative humidity as a function of
337 GHGs during different seasons. Daily mean data is used instead of hourly mean data, to avoid
338 the influence of the diurnal variations on correlations. CO₂ showed a positive correlation with
339 temperature during all season except during winter. This negative correlation can be attributed to
340 different response of photosynthesis rate to different air temperature. IPCC (1990) reports that
341 many mid-latitude plants shows an optimum gross photosynthesis rate when temperature varied
342 from of 20 to 35 °C. The rate of plant respiration tends to be slow below 20°C. However, at
343 higher temperatures, the respiration rate accelerates rapidly up to a temperature at which, it
344 equals the rate of gross photosynthesis and there can be no net assimilation of carbon. While CH₄
345 showed a weak positive correlation with temperature during pre-monsoon and post-monsoon,
346 while a weak negative correlation is observed during monsoon and winter. This could be due to
347 the rate of chemical loss reaction with OH is faster in summer and minimum in other seasons. A
348 case study on CH₄ sink mechanism has discussed in section 4.6. Seasonal variation of GHGs also
349 showed an insignificantly negative correlation with relative humidity. One of the supporting
350 argument can be in humid conditions, these stoma can fully open to increase the uptake of CO₂

351 without a net water loss. Also, wetter soils can promote decomposition of dead plant materials,
352 releasing natural fertilizers that help plants grow (Abhishek et al., 2014).

353 Figure 8a and 8b illustrates the daily mean variation of GHGs with respect to soil moisture
354 and soil temperature (Top panel represent the seasonal variation of CO₂ w.r.t soil moisture and
355 soil temperature, while bottom panel represent the seasonal variation of CH₄ against the same
356 parameters). It's quite interesting to observe that GHGs behave differently w.r.t soil moisture
357 during different seasons. CH₄ shows a positive relationship during monsoon and post-monsoon
358 and an inverse relationship exist during pre-monsoon and winter; while a reverse relationship
359 exist for CO₂. During wet season aeration is restricted (Smith et al. 2003) hence soil respiration
360 is limited, which decrease CO₂ flux. This can be one of the factors for low values of CO₂ during
361 monsoon months, during dry months soil may act as sink of CH.

362 ***4.5.1 Influence of boundary layer height on GHGs mixing ratios***

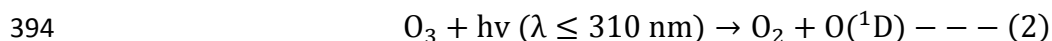
363 The planetary boundary layer is the lowest layer of the troposphere where wind speed as a
364 function of temperature plays major role in its thickness variation. It is an important parameter
365 for controlling the observed diurnal variations and potentially masking the emissions signal
366 (Newman et al., 2013). Since complete set of COSMIC RO data is not available during the study
367 period, in this analysis we have analysed RO data from July 2013 to June 2014, along with
368 simultaneous observations of GHGs. Monthly variations (Figure not show) of BLH computed
369 from high vertical resolution of COSMIC-RO data against CO₂ and CH₄ concentrations.
370 Monthly BLH is observed to be minimum (maximum) during winter and monsoon (pre
371 monsoon) seasons and it closely resembles with the air temperature pattern. The highest (lowest)
372 BLH over study region was identified 3.20 km (1.50 km). A monthly average air temperature is
373 maximum (minimum) of 29°C (20°C) during the summer (winter) months.

374 Seasonal BLH during winter, pre-monsoon, monsoon and post monsoon are 2.10 km, 3.15
375 km, 1.74 km and 2.30 km respectively. Its influence on CO₂ and CH₄ mixing ratios are shown in
376 Figure 9a and 9b. X axis represents the seasonal transition i.e. monsoon to post monsoon (M-
377 PM) etc and y axis indicates seasonal difference of BLH and GHGs concentration respectively.
378 As seasonal BLH increase, mixing ratios of CO₂ (CH₄) decreased from 8.68 ppm to 5.86 ppm
379 (110 ppb to 40 ppb). This effect clearly captured by seasonal diurnal averaged BLH data sets

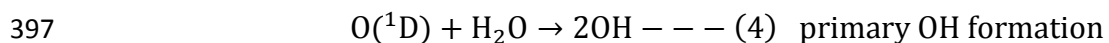
380 used from ECMWF-ERA. The amount of biosphere emissions influence on CO₂ and CH₄ can be
381 estimated through atmospheric boundary layer processes. Since the study region being a flat
382 terrain, variations in CO₂ and CH₄ were mostly influenced by BLH through convection and
383 biosphere activities.

384 **4.6 Methane (CH₄) sink mechanism**

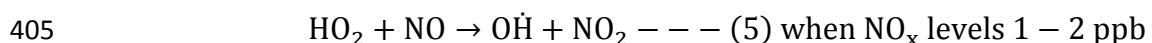
385 Methane (CH₄) is the most powerful greenhouse gas after CO₂ in the atmosphere due to
386 its strong positive radiative forcing (IPCC, AR5). Atmospheric CH₄ is mainly (70-80%) from
387 biological origin produced in anoxic environments, by anaerobic digestion of organic matter
388 (Crutzen and Zimmermann, 1991). The major CH₄ sink is oxidation by hydroxyl radicals (OH),
389 which accounts for 90 % of CH₄ sink (Vaghjiani and Ravishankara, 1991; Kim et al., 2015). OH
390 radicals are very reactive and are responsible for the oxidation of almost all gases in the
391 atmosphere. Primary source for OH radical formation in the atmosphere is photolysis of ozone
392 (O₃) and water vapor (H₂O). Eisele et al., (1997) defined primary and secondary source of OH
393 radicals in the atmosphere. Primary source of OH radical is as follows;



395 where O(^1D) is electronically excited atom



398 Removal of CH₄ is constrained by the presence of OH radicals in the atmosphere. A 1 min time
399 series analysis of CH₄, NO_x, O₃ and H₂O and associated wind vector for August 2014 to
400 understand the CH₄ chemistry is shown in Figure 10a and Figure 10b. Low NO_x (1-2 ppb) values
401 are shown in horizontal elliptical region of Figure 10a and observed corresponding low CH₄
402 (1.80 ppm) concentrations. The low NO_x in turn produces high OH radicals in the atmosphere
403 due to conversion of HO₂ radical by NO, which removes CH₄ through oxidation process as
404 shown below.



406 $\text{CH}_4 + \text{OH} \rightarrow \text{CH}_3 + \text{H}_2\text{O} - - - (6)$ main CH_4 removal process

407 $\text{NO}_2 + \text{OH} + \text{M} \rightarrow \text{HNO}_3 + \text{M} - - - (7)$ if $\text{NO}_x > 2 \text{ ppb}$ ($\text{OH} \downarrow, \text{CH}_4 \uparrow$)

408 Crutzen and Zimmermann, (1991) and Eisele et al., (1997) observed that at low NO_x (0.5-2.0
409 ppb) levels most HO_x family radicals such as HO_2 and peroxy radicals (RO_2) react with NO to
410 form OH radicals. Therefore OH radicals are much higher in the case of low NO_x . When NO_x
411 levels increase more than 2 ppb, most of the OH radicals react with NO_2 to form nitric acid
412 (HNO_3). In first order, the levels of CH_4 in the atmosphere depend on the levels of NO_x though
413 the production of OH radicals in the atmosphere is still uncertain. Figure 10a and 10b showed
414 high CH_4 , H_2O , O_3 and NO_x during a few days in August 2014. High concentrations of CH_4 ,
415 NO_x and other gases are observed in the eastern direction of study site. Very high NO_x levels
416 above 10 ppb are observed and subsequently CH_4 concentrations also increased to 2.40 ppm
417 from 1.80 ppm. In the eastern direction of study site a national highway and single line broad
418 gauge railway network are present which act as possible sources of NO_x , CH_4 and CO_2 . Increase
419 in emissions of NO_x causes decline in the levels of OH radicals and subsequently observed high
420 CH_4 over the study region.

421

422 ***4.7 Long range circulations***

423 To understand the role of long range circulation, we separated the trajectory into 4 clusters
424 based on their pathway, namely North-East (N-E), North-West (N-W), South-East (S-E), South-
425 West (S-W). The main criterion of trajectory clustering is to minimize the variability among
426 trajectories and maximize variability among clusters. Cluster mean trajectories of air mass (Jose
427 et al., 2015b) and their percentage contribution to the total calculated for each season over the
428 study period at 3 Km altitude are depicted in Figure 11. Majority of air mass trajectories during
429 winter (~44%), pre-monsoon (~64%), monsoon (~80%) and post-monsoon (~41%) are
430 originating from NW parts of the study site. For a comprehensive analysis, percentage
431 occurrences of cluster mean trajectories of air mass over study area during different season at
432 different altitudes are also tabulated in Table 4. During post-monsoon to early pre-monsoon
433 periods which are generally the post-harvest period for some of the crops agriculture residue

434 burning which are quite common in the NW and NE regions part of India (Sharma et al,
435 2010).Our analysis reveals that during this period majority of air mass reaching the study site at
436 different altitudes come from this part of the country.

437 **5. Conclusions**

438 The present study analysed the seasonal variations of atmospheric GHGs (CO₂ and CH₄) and
439 associated prevailing meteorology over Shadnagar, a suburban site of Central India during the
440 period 2014. The salient findings of the study are the following:

- 441 • Irrespective of seasons, major sources for CO₂ are soil respiration and anthropogenic
442 emissions while vegetation acts as a main sink. Whereas the major source and sink for
443 CH₄ are vegetation and presence of hydroxyl (OH) radicals. In addition, boundary layer
444 dynamics and long range transport also plays a vital role on GHGs mixing ratios.
- 445 • The annual mean of CO₂ and CH₄ over the study region are found to be 394±2.92 ppm
446 and 1.92±0.07 ppm ($\mu\pm 1\sigma$) respectively. CO₂ and CH₄ show a significant seasonal
447 variation during the study period. Maximum (Minimum) CO₂ is observed during Pre-
448 monsoon (Monsoon), while CH₄ recorded maximum during post-monsoon and
449 minimum in monsoon. Seasonal analysis of FEER data also showed maximum
450 emission of CO₂ due to biomass burning during pre-monsoon months which indicates
451 the influence of biomass burning on local emissions.
- 452 • CO₂ and CH₄ showed consistent diurnal behavior in spite of their significant seasonal
453 variations, with an observed morning (06:00 IST) maxima, followed by afternoon
454 minima (14:00 IST) and enhancing in the late evening (~22:00 IST).
- 455 • Correlation coefficient (Rs) between wind speed and CO₂ during pre-monsoon,
456 monsoon, post-monsoon and winter is 0.56, 0.32, 0.06 and 0.67 respectively. While for
457 CH₄ it is found be 0.28, 0.71, 0.21, and 0.60 respectively. Negative correlation indicates
458 that the influence of local sources on GHGs, however, poor correlation coefficients
459 during different seasons suggest the role of regional/local transport.
- 460 • CO₂ showed a positive correlation with temperature during all seasons except during
461 winter. Whereas CH₄ showed a weak positive correlation with temperature during pre-

462 monsoon and post-monsoon, while showing a weak negative correlation during
463 monsoon and winter.

- 464 • CO₂ and CH₄ showed a strong positive correlation during winter, pre-monsoon,
465 monsoon and post-monsoon with Rs equal to 0.80, 0.80, 0.61 and 0.72 respectively.
466 This clearly indicates common anthropogenic sources for these gases.

467

468 *Acknowledgment*

469 This work was part of the Atmospheric CO₂ Retrieval and Monitoring (ACRM) under
470 National Carbon Project (NCP) of ISRO-GBP. Authors sincerely acknowledge Mr. Biswadip
471 Gharai, ACSG/ECSA for providing LULC data and to Mr. Mallikarjun, ACSG/ECSA for his
472 support in data collection. We thank D & PQE division of NRSC and Mrs. Sujatha P, ACSG for
473 sharing AWS and boundary layer data. The authors are grateful to the AT-CTM project of ISRO-
474 GBP for providing the O₃ and NO_x analyzers. We would also like to thank HYSPLIT, ECMWF-
475 ERA, MODIS and COSMIC team for providing scientific data sets used in this study. We also
476 thankful to anonymous referees and the editor for providing constructive suggestions which
477 certainly improved the quality of the manuscript.

478

479

480

481

482

483

484

485

486 **References**

487 Ao, C. O., D. E. Waliser, S. K. Chan, J.-L. Li, B. Tian, F. Xie, and A. J. Mannucci (2012),
488 Planetary boundary layer heights from GPS radio occultation refractivity and humidity profiles,
489 J. Geophys. Res., 117, D16117, doi:10.1029/2012JD017598.

490 Aurela M, Lohila A, Tuovinen JP, Hatakka J, Riutta T, Laurila T (2009) Carbon dioxide
491 exchange on a northern boreal fen. Boreal Environment Research 14(4): 699-710

492 D. S. Baer, J. B. Paul, M. Gupta, and A. O’Keefe, “Sensitive absorption measurements in the
493 near-infrared region using off-axis integrated-cavity-output spectroscopy,” Applied Physics B
494 75(2-3), 261–265 (2002). doi: 10.1007/s00340-002-0971-z

495 Berman, E. S., Fladeland, M., Liem, J., Kolyer, R., & Gupta, M. Greenhouse gas analyzer for
496 measurements of carbon dioxide, methane, and water vapor aboard an unmanned aerial vehicle.
497 Sensors and Actuators B: Chemical, 169, 128-135, (2012). doi:10.1016/j.snb.2012.04.036

498 Crutzen, P. J., & Andreae, M. O. Biomass burning in the tropics: Impact on atmospheric
499 chemistry and biogeochemical cycles. Science, 250(4988), 1669-1678, (1990). doi:
500 10.1126/science.250.4988.1669

501 Crutzen, P. J., A. C. Delany, J. Greenberg, P. Haagenson, L. Heidt, R. Lueb, W. Pollock,
502 Wartburg Seiler, A. Wartburg, and P. Zimmerman. "Tropospheric chemical composition
503 measurements in Brazil during the dry season." Journal of Atmospheric Chemistry 2, no. 3
504 (1985): 233-256. doi: 10.1007/BF00051075

505 Crutzen, P. J., & Zimmermann, P. H. (1991). The changing photochemistry of the troposphere.
506 Tellus B, 43(4), 136-151. doi: 10.1034/j.1600-0870.1991.00012.x

507 Crutzen, P. J. (1991). Methane's sinks and sources. Nature, 350, 380-381; doi:10.1038/350380a0.

508

509 Draxler RR, Rolph GD. HySPLIT (Hybrid Single Particle Lagrangian Integrated Trajectory)
510 Model access via NOAA ARL READY website (<http://www.arl.noaa.gov/ready/hysplit4.html>),
511 NOAA Air Resources Laboratory. *Silver Spring, MD*. 2003.

512

513 Eisele, F. L., Mount, G. H., Tanner, D., Jefferson, A., Shetter, R., Harder, J. W., & Williams, E.
514 J. Understanding the production and interconversion of the hydroxyl radical during the
515 Tropospheric OH Photochemistry Experiment. *Journal of Geophysical Research: Atmospheres*
516 (1984–2012), 102(D5), 6457-6465, (1997). doi: 10.1029/96JD02207

517 Fang, S. X., L. X. Zhou, P. P. Tans, P. Ciais, M. Steinbacher, L. Xu, and T. Luan. "In situ
518 measurement of atmospheric CO₂ at the four WMO/GAW stations in China." *Atmospheric*
519 *Chemistry and Physics* 14, no. 5 (2014): 2541-2554. doi: 10.5194/acp-14-2541-2014

520 Fang, S. X., P. P. Tans, M. Steinbacher, L. X. Zhou, and T. Luan. "Study of the regional CO₂
521 mole fractions filtering approach at a WMO/GAW regional station in China." *Atmospheric*
522 *Measurement Techniques Discussions* 8, no. 7 (2015). doi: 10.5194/amt-8-5301-2015

523

524 Frankenberg, Christian, Peter Bergamaschi, André Butz, Sander Houweling, Jan Fokke Meirink,
525 Justus Notholt, Anna Katinka Petersen, Hans Schrijver, Thorsten Warneke, and Ilse Aben.
526 "Tropical methane emissions: A revised view from SCIAMACHY onboard ENVISAT."
527 *Geophysical Research Letters* 35, no. 15 (2008). doi: 10.1029/2008GL034300.

528 Garg, A., Bhattacharya, S., Shukla, P. R., & Dadhwal, V. K. Regional and sectoral assessment of
529 greenhouse gas emissions in India. *Atmospheric Environment*, 35(15), 2679-2695, (2001).

530

531 Gaur, A., Tripathi, S. N., Kanawade, V. P., Tare, V., & Shukla, S. P. Four-year measurements of
532 trace gases (SO₂, NO_x, CO, and O₃) at an urban location, Kanpur, in Northern India. *Journal of*
533 *Atmospheric Chemistry*, 71(4), 283-301, (2014).

534

535 Gilmanov, T. G., Johnson, D. A., Saliendra, N. Z., Akshalov, K., & Wylie, B. K. Gross primary
536 productivity of the true steppe in Central Asia in relation to NDVI: scaling up CO₂ fluxes.
537 *Environmental Management*, 33(1), S492-S508, (2004).

538 Goroshi, S. K., Singh, R. P., Panigrahy, S., & Parihar, J. S. Analysis of seasonal variability of
539 vegetation and methane concentration over India using SPOT-VEGETATION and ENVISAT-
540 SCIAMACHY data. *Journal of the Indian Society of Remote Sensing*, 39(3), 315-321, (2011).
541

542 Hassan, A. G. A. Diurnal and Monthly Variations in Atmospheric CO₂ Level in Qena, Upper
543 Egypt. *Resources and Environment*, 5(2), 59-65, (2015).
544

545 Hayashida, S., Ono, A., Yoshizaki, S., Frankenberg, C., Takeuchi, W., & Yan, X. (2013).
546 Methane concentrations over Monsoon Asia as observed by SCIAMACHY: Signals of methane
547 emission from rice cultivation. *Remote Sensing of Environment*, 139, 246-256.
548

549 Huang, J. P., W. Zhang, J. Q. Zuo, J. R. Bi, J. S. Shi, X. Wang, Z. L. Chang, Z. W. Huang, S.
550 Yang, B. D. Zhang, G. Y. Wang, G. H. Feng, J. Y. Yuan, L. Zhang, H. C. Zuo, S. G. Wang, C.
551 B. Fu, and J. F. Chou, 2008: An overview of the semi-arid climate and environment research
552 observatory over the Loess Plateau. *Advances in Atmospheric Sciences.*, 25(6), 906–921, doi:
553 10.1007/s00376-008-0906-7.
554

555 Huang, J., Yu, H., Guan, X., Wang, G., & Guo, R. (2015). Accelerated dryland expansion under
556 climate change. *Nature Climate Change*, doi: 10.1038/nclimate2837.

557 Ichoku, C., & Ellison, L. Global top-down smoke-aerosol emissions estimation using satellite
558 fire radiative power measurements. *Atmospheric Chemistry and Physics*, 14(13), 6643-6667,
559 (2014). doi:10.5194/acp-14-6643-2014

560 Intergovernmental Panel on Climate Change (IPCC). *Climate Change: The IPCC Scientific*
561 *Assessment*, edited by J. T. Houghton, G. J. Jerkins and J. J. Ephraums. Cambridge University
562 Press. New York, (IPCC, 1990).

563 James, M. E., & Kalluri, S. N. The Pathfinder AVHRR land data set: an improved coarse
564 resolution data set for terrestrial monitoring. *International Journal of Remote Sensing*, 15(17),
565 3347-3363, (1994). DOI: 10.1080/01431169408954335

566 Jing, X., Huang, J., Wang, G., Higuchi, K., Bi, J., Sun, Y., & Wang, T. (2010). The effects of
567 clouds and aerosols on net ecosystem CO₂ exchange over semi-arid Loess Plateau of Northwest
568 China. *Atmospheric Chemistry and Physics*, 10(17), 8205-8218. doi:10.5194/acp-10-8205-2010

569 Jones, C., McConnell, C., Coleman, K., Cox, P., Falloon, P., Jenkinson, D., & Powlson, D.
570 Global climate change and soil carbon stocks; predictions from two contrasting models for the
571 turnover of organic carbon in soil. *Global Change Biology*, 11(1), 154-166, (2005). doi:
572 10.1111/j.1365-2486.2004.00885.x

573

574 Jose, S., Gharai, B., Kumar, Y. B., & Rao, P. V. N. (2015a). Radiative implication of a haze
575 event over Eastern India. *Atmospheric Pollution Research*, 6(1), 138-146.
576 doi:10.5094/APR.2015.016

577

578 Jose, S., K. Niranjana, Biswadip Gharai, and P.V.N Rao. (2015b). Characterisation of absorbing
579 aerosols using ground and satellite data at an urban location, Hyderabad. *Aerosol and air quality*
580 *research*. doi: 10.4209/aaqr.2014.09.0220

581 Kepler, F., Hamilton, J. T., Braß, M., & Röckmann, T. Methane emissions from terrestrial
582 plants under aerobic conditions. *Nature*, 439(7073), 187-191, (2006). doi:10.1038/nature04420;

583 Kim, H. S., Chung, Y. S., Tans, P. P., & Dlugokencky, E. J. Decadal trends of atmospheric
584 methane in East Asia from 1991 to 2013. *Air Quality, Atmosphere & Health*, 8(3), 293-298,
585 (2015). doi: 10.1007/s11869-015-0331-x

586 King, M. D., Kaufman, Y. J., Menzel, W. P., & Tanre, D. Remote sensing of cloud, aerosol, and
587 water vapor properties from the Moderate Resolution Imaging Spectrometer (MODIS).
588 *Geoscience and Remote Sensing, IEEE Transactions on*, 30(1), 2-27, (1992). doi:
589 10.1109/36.124212

590 Kirschke, Stefanie., Bousquet, Philippe., Ciais, Philippe., Saunois, Marielle., Canadell, Josep G.,
591 Dlugokencky, Edward J., Bergamaschi, Peter., Bergmann, Daniel., Blake, Donald R., Bruhwiler,
592 Lori., Cameron-Smith, Philip., Castaldi, Simona., Chevallier, Frédéric., Feng, Liang., Fraser,
593 Annemarie., Heimann, Martin., Hodson, Elke L., Houweling, Sander., Josse, Béatrice., Fraser,
594 Paul J., Krummel, Paul B., Lamarque, Jean-François., Langenfelds, Ray L., Quéré, Corinne Le.,
595 Naik, Vaishali., O'Doherty, Simon., Palmer, Paul I., Pison, Isabelle., Plummer, David., Poulter,
596 Benjamin., Prinn, Ronald G., Rigby, Matt., Ringeval, Bruno., Santini, Monia., Schmidt,
597 Martina., Shindell, Drew T., Simpson, Isobel J., Spahni, Renato., Steele, L. Paul., Strode, Sarah
598 A., Sudo, Kengo., Szopa, Sophie., Werf, Guido R. van der., Voulgarakis, Apostolos., Wee,
599 Michiel van., Weiss, Ray F., Williams, Jason E., Guang, Zeng. Three decades of global methane
600 sources and sinks, *Nature Geoscience*, volume 6, (2013), doi: 10.1038/NNGEO1955.

601 Koshal. A. K. Spatial temporal climatic change variability of cropping system in western Uttar
602 Pradesh, *International Journal of Remote Sensing & Geoscience*, volume 2, issue 3, (2013).

603 Lewis, A. C., Evans, M. J., Hopkins, J. R., Punjabi, S., Read, K.A., Purvis, R. M., Andrews, S.
604 J., Moller, S. J., Carpenter, L.J., Lee, J. D., Rickard, A. R., Palmer, P. I., and Parrington, M.: The
605 influence of biomass burning on the global distribution of selected non-methane organic
606 compounds, *Atmos. Chem. Phys.*, 13, 851–867, doi:10.5194/acp-13-851-2013, 2013.

607 Liu, Yang, Xiufeng Wang, Meng Guo, Hiroshi Tani, Nobuhiro Matsuoka, and Shinji
608 Matsumura. "Spatial and temporal relationships among NDVI, climate factors, and land cover
609 changes in Northeast Asia from 1982 to 2009." *GIScience & Remote Sensing* 48, no. 3 (2011):
610 371-393. doi: 10.2747/1548-1603.48.3.371

611

612 Machida, T., K. Kita, Y. Kondo, D. Blake, S. Kawakami, G. Inoue, and T. Ogawa, Vertical and
613 meridional distributions of the atmospheric CO₂ mixing ratio between northern midlatitudes and
614 southern subtropics, *Journal of Geophysical Research.*, 107, 8401, doi:10.1029/2001JD000910,
615 2002.

616 Mahesh, P., N. Sharma, V. K. Dadhwal, P. V. N. Rao, and B. V. Apparao. "Impact of Land-Sea
617 Breeze and Rainfall on CO₂ Variations at a Coastal Station. *J Earth Sci Clim Change* 5: 201. doi:
618 10.4172/2157-7617.1000201 Volume 5. Issue 6. (2014).

619 Mahesh. P, Sreenivas. G, Rao.P.V.N., Dadhwal.V.K.,Sai Krishna. S.V.S. and Mallikarjun. K:
620 High precision surface level CO₂ and CH₄ using Off-Axis Integrated Cavity Output
621 Spectroscopy (OA-ICOS) over Shadnagar, India, *International Journal of Remote Sensing*,
622 (2015), doi:10.1080/01431161.2015.1104744.

623 Miller, John B., Luciana V. Gatti, Monica TS d'Amelio, Andrew M. Crotwell, Edward J.
624 Dlugokencky, Peter Bakwin, Paulo Artaxo, and Pieter P. Tans. "Airborne measurements indicate
625 large methane emissions from the eastern Amazon basin." *Geophysical Research Letters* 34, no.
626 10 (2007). doi/10.1029/2006GL029213.

627 Monastersky, Richard. "Global carbon dioxide levels near worrisome milestone." *Nature* 497,
628 no. 7447 (2013): 13-14. doi: 10.1038/497013a.

629 Newman, S., Jeong, S., Fischer, M. L., Xu, X., Haman, C. L., Lefer, B., Alvarez,
630 S.,Rappenglueck, B.,Kort, E. A., Andrews, A. E., Peischl, J.,Gurney, K. R.,Miller, C. E.,and
631 Yung, Y. L.,: Diurnal tracking of anthropogenic CO₂ emissions in the Los Angeles basin
632 megacity during spring, *Atmos. Chem. Phys.*, 13, 4359–4372, 2013, doi:10.5194/acp-13-4359-
633 2013.

634 Nishanth, T., K. M. Praseed, M. K. Satheesh Kumar, and K. T. Valsaraj. "Observational study of
635 surface O₃, NO_x, CH₄ and total NMHCs at Kannur, India." *Aerosol. Air. Qual. Res* 14 (2014):
636 1074-1088 doi: 10.4209/aaqr.2012.11.0323.

637 Pan, X. L., Kanaya, Y., Wang, Z. F., Liu, Y., Pochanart, P., Akimoto, H., Sun, Y. L., Dong, H.
638 B., Li, J., Irie, H., and Takigawa, M.: Correlation of black carbon aerosol and carbon monoxide
639 in the high-altitude environment of Mt. Huang in Eastern China, *Atmos. Chem. Phys.*, 11, 9735-
640 9747, doi:10.5194/acp-11-9735-2011, 2011

641 Paul, J. B., Lapson, L., & Anderson, J. G.. Ultrasensitive absorption spectroscopy with a high-
642 finesse optical cavity and off-axis alignment. *Applied Optics*, 40(27), 4904-4910, (2001). doi:
643 10.1364/AO.40.004904

644 Patil, M. N., T. Dharmaraj, R. T. Waghmare, T. V. Prabha, and J. R. Kulkarni. "Measurements of
645 carbon dioxide and heat fluxes during monsoon-2011 season over rural site of India by eddy
646 covariance technique." *Journal of Earth System Science* 123, no. 1 (2014): 177-185. doi:
647 10.1007/s12040-013-0374-z

648 Pielke, Roger A., Gregg Marland, Richard A. Betts, Thomas N. Chase, Joseph L. Eastman, John
649 O. Niles, and Steven W. Running. "The influence of land-use change and landscape dynamics on
650 the climate system: relevance to climate-change policy beyond the radiative effect of greenhouse
651 gases." *Philosophical Transactions of the Royal Society of London A: Mathematical, Physical
652 and Engineering Sciences* 360, no. 1797 (2002): 1705-1719. doi: 10.1098/rsta.2002.1027

653 Ramachandran, S., and T. A. Rajesh. "Black carbon aerosol mass concentrations over
654 Ahmedabad, an urban location in western India: comparison with urban sites in Asia, Europe,
655 Canada, and the United States." *Journal of Geophysical Research: Atmospheres* (1984–2012)
656 112, no. D6 (2007). doi/10.1029/2006JD007488.

657

658 Salomonson, Vincent V., W. L. Barnes, Peter W. Maymon, Harry E. Montgomery, and Harvey
659 Ostrow. "MODIS: Advanced facility instrument for studies of the Earth as a system."
660 *Geoscience and Remote Sensing, IEEE Transactions on* 27, no. 2 (1989): 145-153. doi:
661 10.1109/36.20292

662 Smith, K. A., Ball, T., Conen, F., Dobbie, K. E., Massheder, J., & Rey, A. Exchange of
663 greenhouse gases between soil and atmosphere: interactions of soil physical factors and
664 biological processes. *European Journal of Soil Science*, 54(4), 779-791, (2003), doi:
665 10.1046/j.1351-0754.2003.0567.x

666 Schneising, O., M. Buchwitz, J. P. Burrows, H. Bovensmann, P. Bergamaschi, and W. Peters.
667 "Three years of greenhouse gas column-averaged dry air mole fractions retrieved from satellite—
668 Part 2: Methane." *Atmos. Chem. Phys* 9, no. 2 (2009): 443-465, doi:10.5194/acp-9-443-2009

669 Sharma Neerja, Dadhwal, V.K., Kant, Y., Mahesh, P., Mallikarjun, K., Gadavi, Harish, Sharma,
670 Anand., Ali, M.M. Atmospheric CO₂ Variations in Two Contrasting Environmental Sites Over
671 India. *Air, Soil and Water Research* 2014:7 61–68, (2014), doi:10.4137/ASWR.S13987.

672 Sharma, Anu Rani, Shailesh Kumar Kharol, K. V. S. Badarinath, and Darshan Singh. "Impact of
673 agriculture crop residue burning on atmospheric aerosol loading—a study over Punjab State,
674 India." In *Annales geophysicae: atmospheres, hydrospheres and space sciences*, vol. 28, no. 2, p.
675 367. 2010. www.ann-geophys.net/28/367/2010/

676 Sharma, Neerja, Rabindra K. Nayak, Vinay K. Dadhwal, Yogesh Kant, and Meer M. Ali.
677 "Temporal variations of atmospheric CO₂ in Dehradun, India during 2009." *Air, Soil and Water*
678 *Research* 6 (2013): 37, doi: 10.4137/ASWR.S10590.

679 Stocker, T.F., Qin, D., Plattner, G.K., Alexander, L.V., Allen, S.K., Bindoff, N.L., Bréon, F.M.,
680 Church, J.A., Cubasch, U., Emori, S., Forster, P., Friedlingstein, P., Gillett, N., Gregory, J.M.,
681 Hartmann, D.L., Jansen, E., Kirtman, B., Knutti, R., Krishna Kumar, K., Lemke, P., Marotzke,
682 J., Masson-Delmotte, V., Meehl, G.A., Mokhov, I.I., Piao, S., Ramaswamy, V., Randall, D.,
683 Rhein, M., Rojas, M., Sabine, C., Shindell, D., Talley, L.D., Vaughan D.G., and Xie, S.P.
684 Technical Summary. In: *Climate Change 2013: The Physical Science Basis. Contribution of*
685 *Working Group I to the Fifth Assessment Report of the Intergovernmental Panel on Climate*
686 *Change* [Stocker, T.F., D. Qin, G.-K. Plattner, M. Tignor, S.K. Allen, J. Boschung, A. Nauels, Y.
687 Xia, V. Bex and P.M. Midgley (eds.)]. Cambridge University Press, Cambridge, United
688 Kingdom and New York, NY, USA, (2013).Shea, S.J.O, G. Allen¹, M. W. Gallagher, S. J.-B.
689 Bauguitte, S. M. Illingworth, M. Le Breton, J. B. A. Muller,C. J. Percival, A. T. Archibald, D. E.
690 Oram, M. Parrington,^{*} P. I. Palmer, and A. C. Lewis. Airborne observations of trace gases over
691 boreal Canada during BORTAS: campaign climatology, air mass analysis and enhancement
692 ratios. *Atmos. Chem. Phys.*, 13, 12451–12467, 2013 atmos-chem-phys.net/13/12451/2013/
693 doi:10.5194/acp-13-12451-2013

694 Stohl, Andreas, Markus Hittenberger, and Gerhard Wotawa. "Validation of the Lagrangian
695 particle dispersion model FLEXPART against large-scale tracer experiment data." *Atmospheric*
696 *Environment* 32, no. 24 (1998): 4245-4264, doi:10.1016/S1352-2310(98)00184-8.

697
698 Stull, R. B. (1988). *Similarity theory*. In *An Introduction to Boundary Layer Meteorology* (pp.
699 347-404). Springer Netherlands.

700 Taylor J. *An Introduction to Error Analysis: The Study of Uncertainties in Physical*
701 *Measurement*, University Science Books, And ISBN: 093570275X (ISBN13: 9780935702750),
702 (1997).

703 Thum, T., T. Aalto, T. Laurila, M. Aurela, J. Hatakka, Anders Lindroth, and T. Vesala. "Spring
704 initiation and autumn cessation of boreal coniferous forest CO₂ exchange assessed by
705 meteorological and biological variables." *Tellus B* 61, no. 5 (2009): 701-717,doi:
706 10.1111/j.1600-0889.2009.00441.x.

707 Tohjima, Y., Kubo, M., Minejima, C., Mukai, H., Tanimoto, H., Ganshin, A., Maksyutov, S.,
708 Katsumata, K., Machida, T., and Kita, K.: Temporal changes in the emissions of CH₄ and CO
709 from China estimated from CH₄ / CO₂ and CO / CO₂ correlations observed at Hateruma Island,
710 *Atmos. Chem. Phys.*, 14, 1663-1677, doi:10.5194/acp-14-1663-2014, 2014.

711
712 Vaghjiani, Ghanshyam L., and A. R. Ravishankara. "New measurement of the rate coefficient
713 for the reaction of OH with methane." *Nature* 350, no. 6317 (1991): 406-409; doi:
714 10.1038/350406a0.

715 Wang, B-R., X-Y. Liu, and J-K. Wang. "Assessment of COSMIC radio occultation retrieval
716 product using global radiosonde data." *Atmospheric Measurement Techniques* 6, no. 4 (2013):
717 1073-1083; doi:10.5194/amt-6-1073-2013.

718 Wang, G., J. Huang*, W. Guo, J. Zuo, J. Wang, J. Bi, Z. Huang, and J. Shi, 2010: Observation
719 analysis of land-atmosphere interactions over the Loess Plateau of northwest China, *J. Geophys.*
720 *Res.*, 115, D00K17, doi:10.1029/2009JD013372.

721 Worthy, D. E. J., E. Chan, M. Ishizawa, D. Chan, C. Poss, E. J. Dlugokencky, S. Maksyutov,
722 and I. Levin (2009), Decreasing anthropogenic methane emissions in Europe and Siberia inferred
723 from continuous carbon dioxide and methane observations at Alert, Canada, *Journal of*
724 *Geophysical Research.*, 114, D10301, doi:10.1029/2008JD011239.

725 Yunck, Thomas P., Liu Chao-Han, and Randolph Ware. "A history of GPS sounding."
726 *Terrestrial Atmospheric and Oceanic Sciences* 11, no. 1 (2000): 1-20, doi: 10.5772/6928.

727
728
729
730
731
732
733
734
735
736
737
738
739
740
741
742
743
744
745
746
747
748
749
750
751
752

753 **Table 1** Data used

754

| Sensor | Period | Parameter | resolution | Source |
|---|-------------------------|--|--|---|
| GGA-24EP | Jan-2014 to Dec 2014 | CO ₂ ,CH ₄ and H ₂ O | 1 Hz time | ASL,NRSC |
| 42i-NO- NO ₂ -NO _x | Jul-2014 to Sep-2014 | NO _x (=NO+N O ₂) | 1 min time | ASL,NRSC |
| 49i-O ₃ | Jul-2014 to Sep-2014 | O ₃ | 1 min time | ASL,NRSC |
| AWS | Jan-2014 to Dec-2014 | WS,WD,AT,R H | 60 min time | NRSC |
| Terra/MODI S | Jan-2014 to Dec-2014 | NDVI | 5 Km horizontal | http://ladsweb.nascom.nasa.gov/data/search.html |
| COSMIC- 1DVAR | Jul-2013 to Jun-2014 | Refractivity (N) | 0.1 Km vertical | |
| HYSPLIT | Jan-2014 to Dec-2014 | Backward trajectory | 5 day isentropic model (1km to 4 km) | http://ww.arl.noaa.gov/ready/hysplit4.html |
| FEER v1 | Jan-2013 to Dec-2013 | fire radiative power (FRP) | | http://ladsweb.nascom.nasa.gov/data/search.html |

755

756

757

758

759

760

761

762

763

764

765 **Table 2** Statistical correlation between CO₂ and CH₄

766
767
768
769
770
771
772
773
774
775
776
777
778
779
780
781
782
783
784

| S.No | Seasons | Correlation coefficient (R) | Slope $\left(\frac{Y_{CH_4} (ppm)}{X_{CO_2} (ppm)}\right)$ | Ψ_{slope} (ppm) | Ψ_{y-int} (ppm) |
|------|--------------------|-----------------------------|--|----------------------|----------------------|
| 1 | Monsoon (JJAS) | 0.61 | 0.005 | 0.00015 | 1.91 |
| 2 | Post-monsoon (OND) | 0.72 | 0.0065 | 0.00014 | 1.52 |
| 3 | Winter (JF) | 0.80 | 0.0085 | 0.00018 | 9.13 |
| 4 | Pre-monsoon (MAM) | 0.80 | 0.0059 | 0.00021 | 2.73 |

785

786 **Table 3** Seasonal amplitudes of CO₂ and CH₄ over study region arriving from different

787 directions

| Wind Direction | Winter $\frac{\text{CO}_2}{\text{CH}_4}$ (ppm) | Pre-monsoon $\frac{\text{CO}_2}{\text{CH}_4}$ (ppm) | Monsoon $\frac{\text{CO}_2}{\text{CH}_4}$ (ppm) | Post-monsoon $\frac{\text{CO}_2}{\text{CH}_4}$ (ppm) |
|----------------|---|--|--|---|
| 0-45 | 399.85/1.98 | 410.37/1.94 | 400.72/1.91 | 395.13/2.02 |
| 45-90 | 391.66/1.94 | 399.59/1.89 | 388.82/1.91 | 390.23/1.98 |
| 90-135 | 391.57/1.93 | 397.79/1.87 | 388.99/1.87 | 389.06/1.97 |
| 135-180 | 389.34/1.89 | 393.87/1.85 | 391.81/1.86 | 387.69/1.97 |
| 180-225 | 391.14/1.89 | 396.75/1.85 | 390.28/1.82 | 392.30/2.02 |
| 225-270 | 389.13/1.88 | 394.81/1.86 | 390.26/1.82 | 384.40/1.94 |
| 270-315 | 388.68/1.87 | 398.68/1.89 | 389.58/1.82 | 384.99/1.93 |
| 315-360 | 390.87/1.91 | 401.17/1.89 | 387.58/1.83 | 389.32/1.98 |

788

789

790

791

792

793

794

795

796

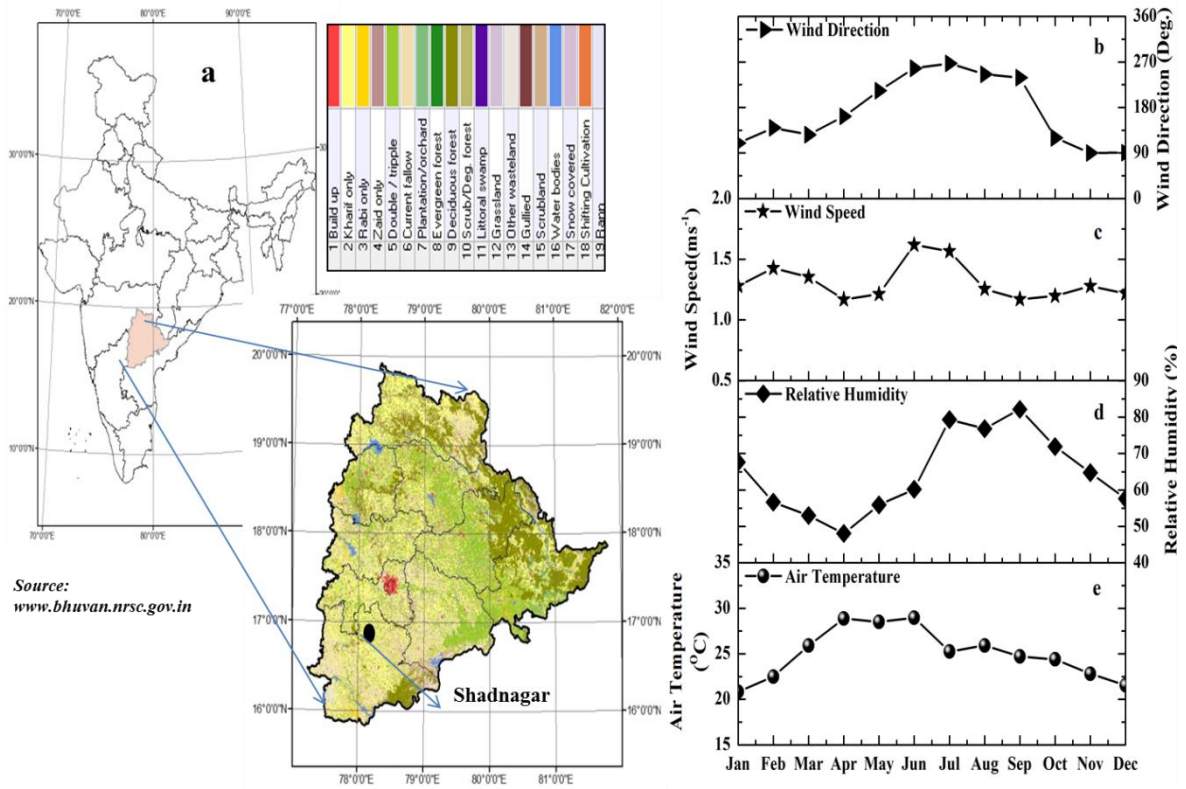
797

798

799 **Table 4** Cluster analysis of air mass trajectories reaching Shadnagar at various heights during
 800 different seasons

| Seasonal Backward trajectory (%) | NW | | | | NE | | | | SE | | | | SW | | | |
|---|---------|---------|---------|---------|---------|---------|---------|---------|---------|---------|---------|---------|---------|---------|---------|---------|
| | 1 km | 2 km | 3 km | 4 km | 1 km | 2 km | 3 km | 4 km | 1 km | 2 km | 3 km | 4 km | 1 km | 2 km | 3 km | 4 km |
| Winter | 54 | 32 | 2 | 0 | 32 | 24 | 44 | 52 | 10 | 25 | 11 | 7 | 4 | 19 | 42 | 41 |
| Pre-monsoon | 24 | 9 | 8 | 1 | 26 | 31 | 64 | 78 | 36 | 46 | 2 | 10 | 14 | 14 | 26 | 11 |
| Monsoon | 0 | 1 | 7 | 19 | 12 | 34 | 80 | 70 | 4 | 4 | 4 | 6 | 84 | 61 | 9 | 5 |
| Post- monsoon | 42 | 15 | 11 | 14 | 47 | 53 | 41 | 49 | 8 | 30 | 32 | 26 | 3 | 2 | 16 | 11 |

801
 802
 803
 804
 805
 806
 807
 808
 809
 810
 811
 812
 813



814

815

816

817 **Figure 1** a) Schematic representation of study area; b-e) Seasonal variation of prevailing
 818 meteorological conditions during 2014

819

820

821

822

823

824

825

826

827

828

829

830

831

832

833

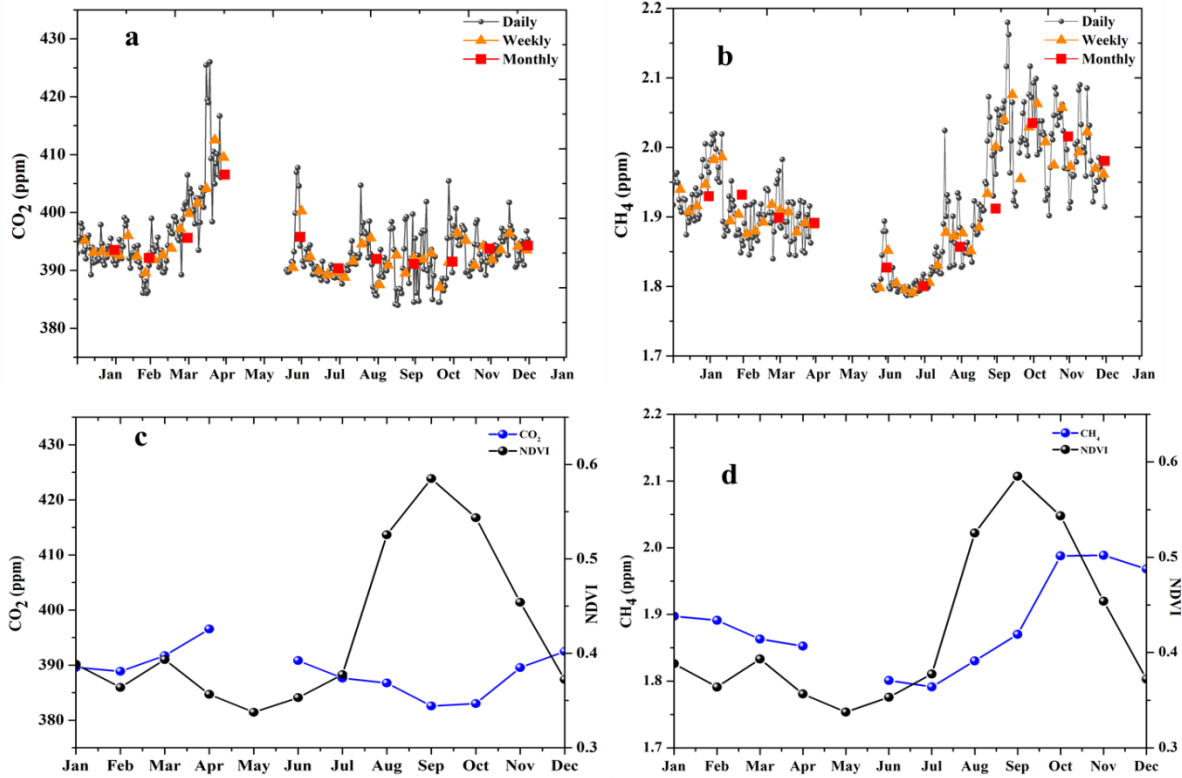
834

835

836

837

838



839 **Figure 2** a-b) Temporal variations of CO₂ and CH₄; c-d) Seasonal variations of CO₂ and CH₄ in
840 conjunction with NDVI (Normalized Difference Vegetation Index) during 2014

841

842

843

844

845

846

847

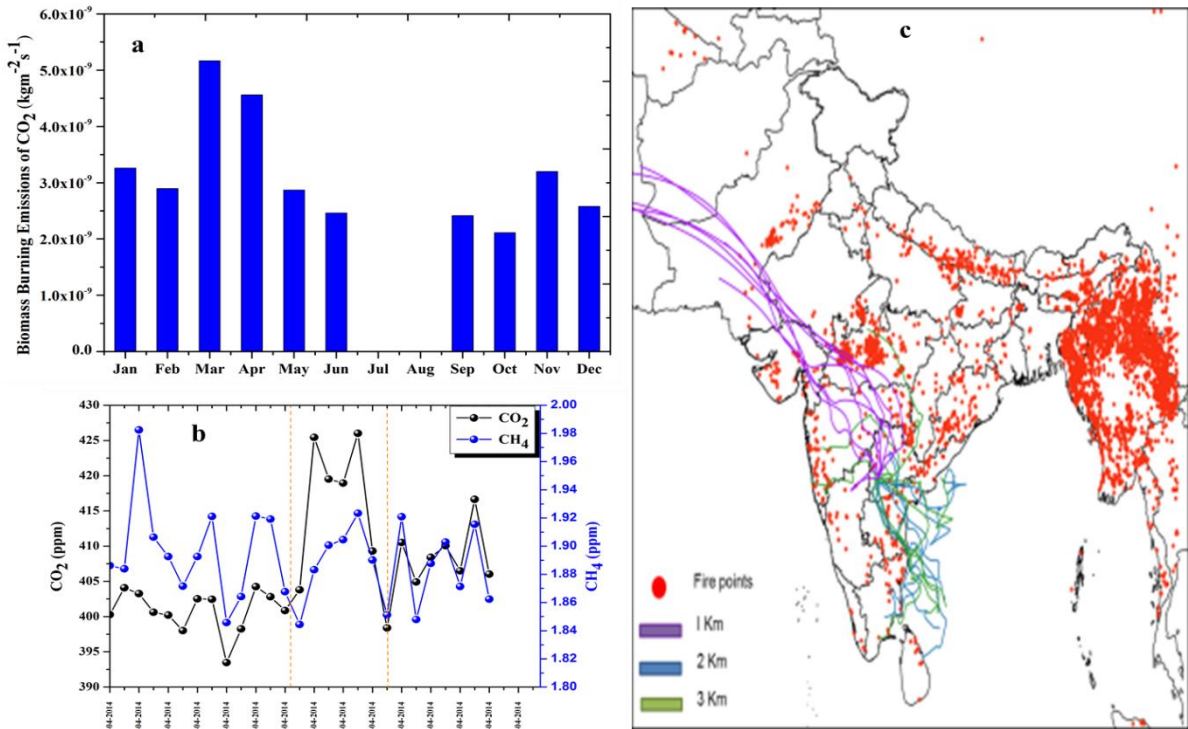
848

849

850

851

852



853 **Figure 3** a) Long term analysis of CO₂ biomass burning emissions over study region b) Biomass
 854 signatures on CO₂/CH₄ during 14-21 April 2014, a case study c) Spatial distribution of MODIS
 855 derived fire counts over Indian region during 14-21 April 2014.

856

857

858

859

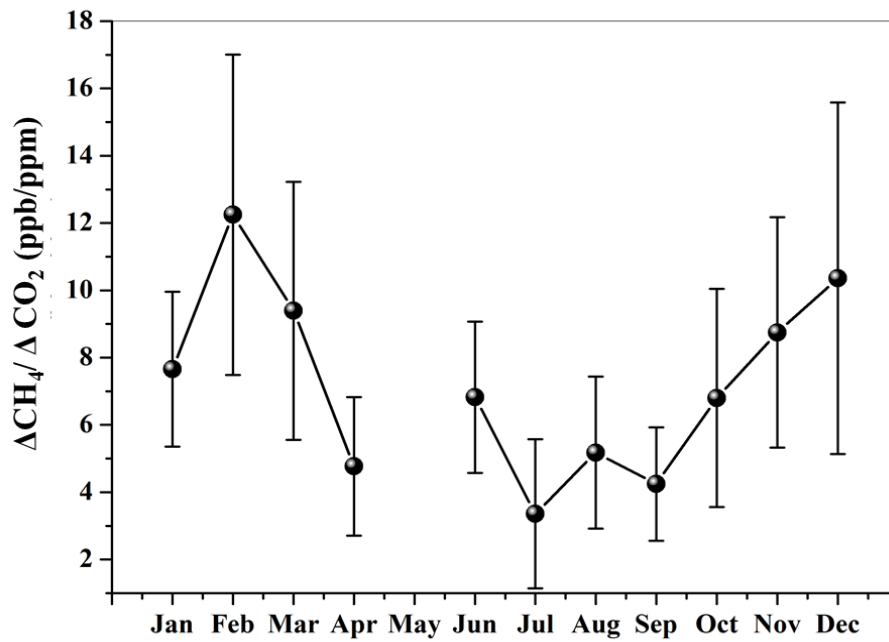
860

861

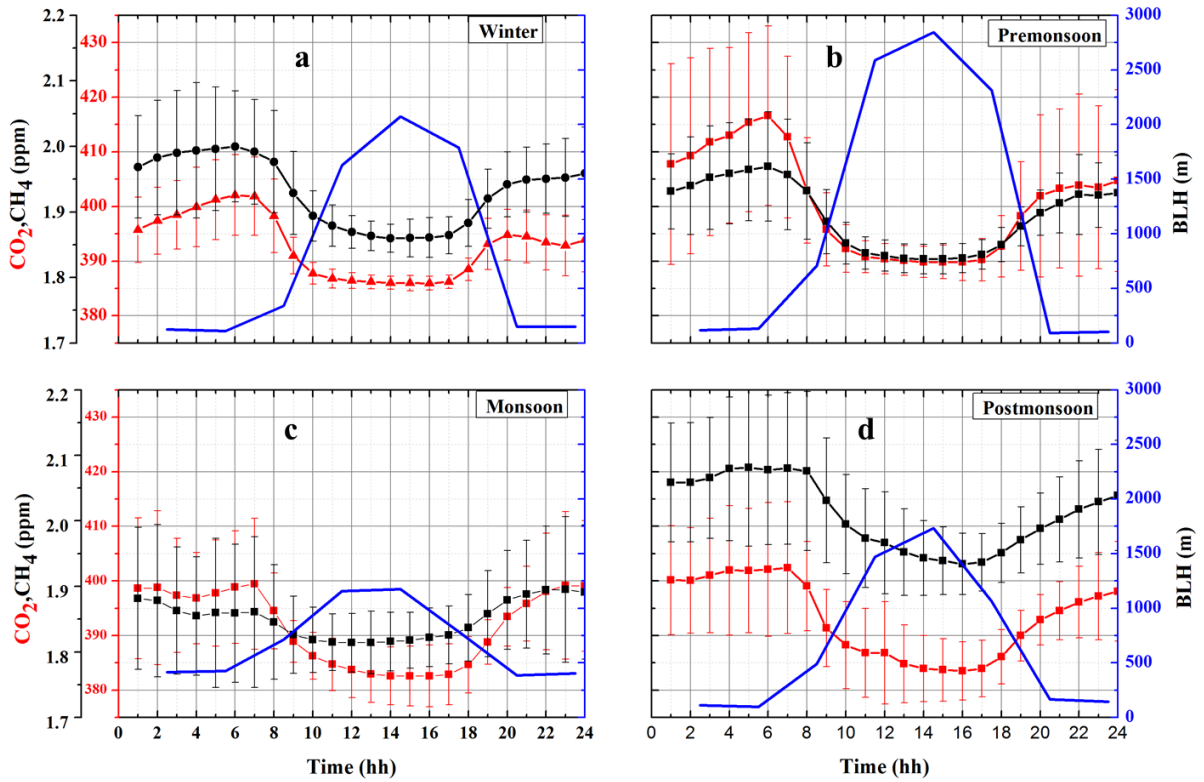
862

863

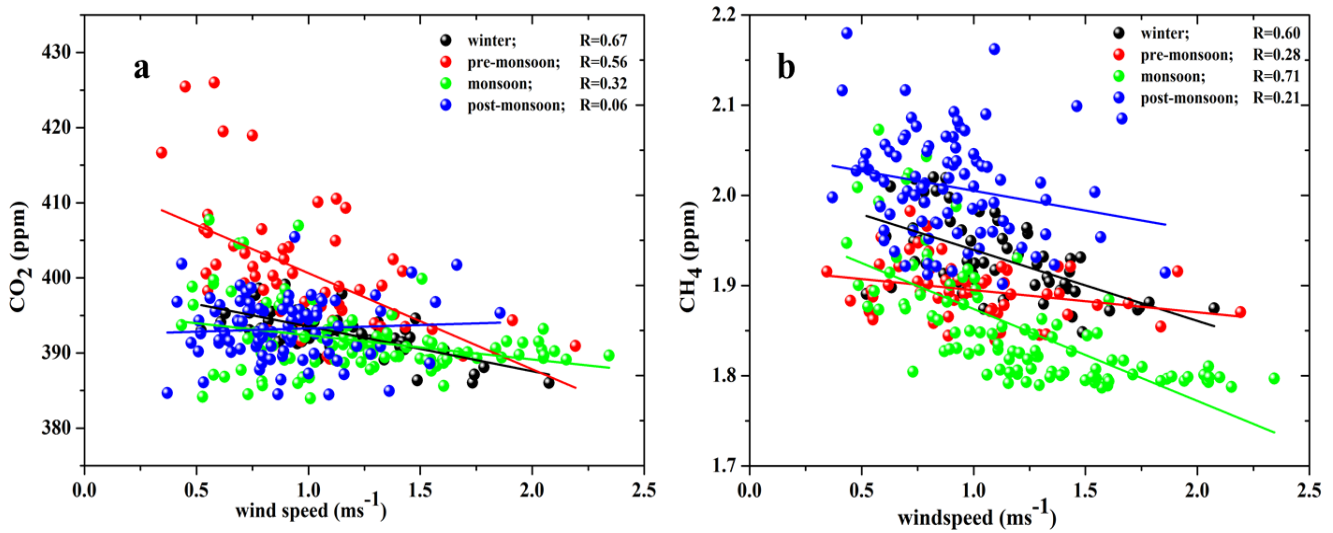
864



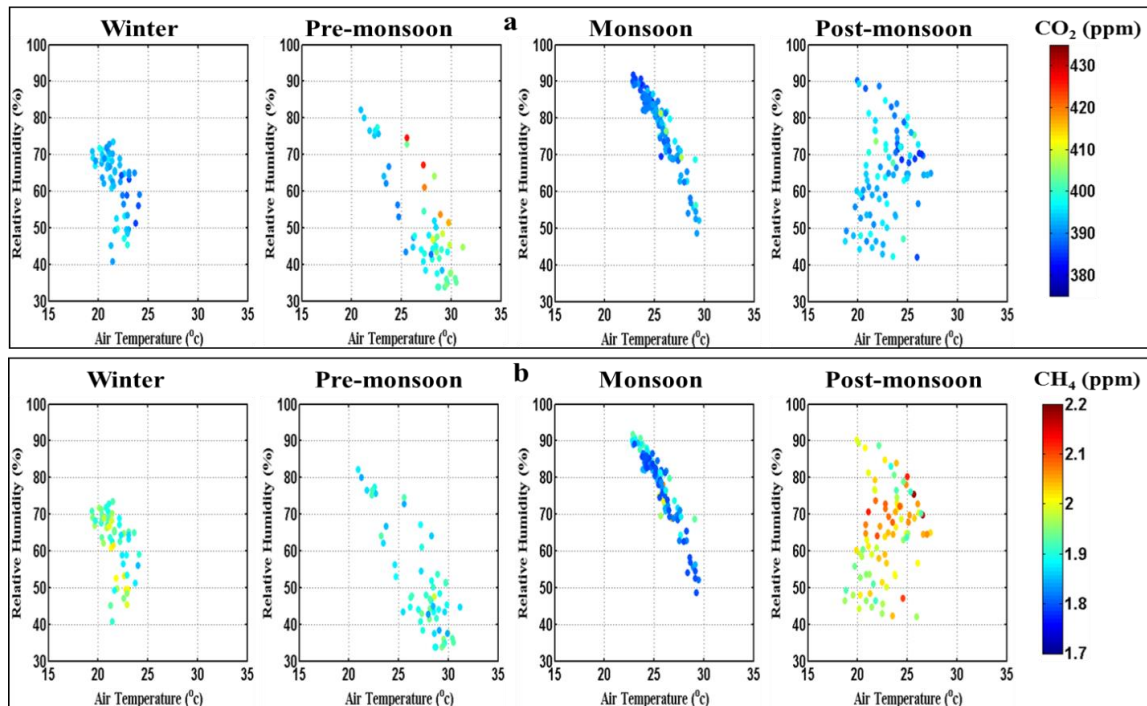
865 **Figure 4** Monthly variation of $\Delta\text{CH}_4/\Delta\text{CO}_2$ during study period



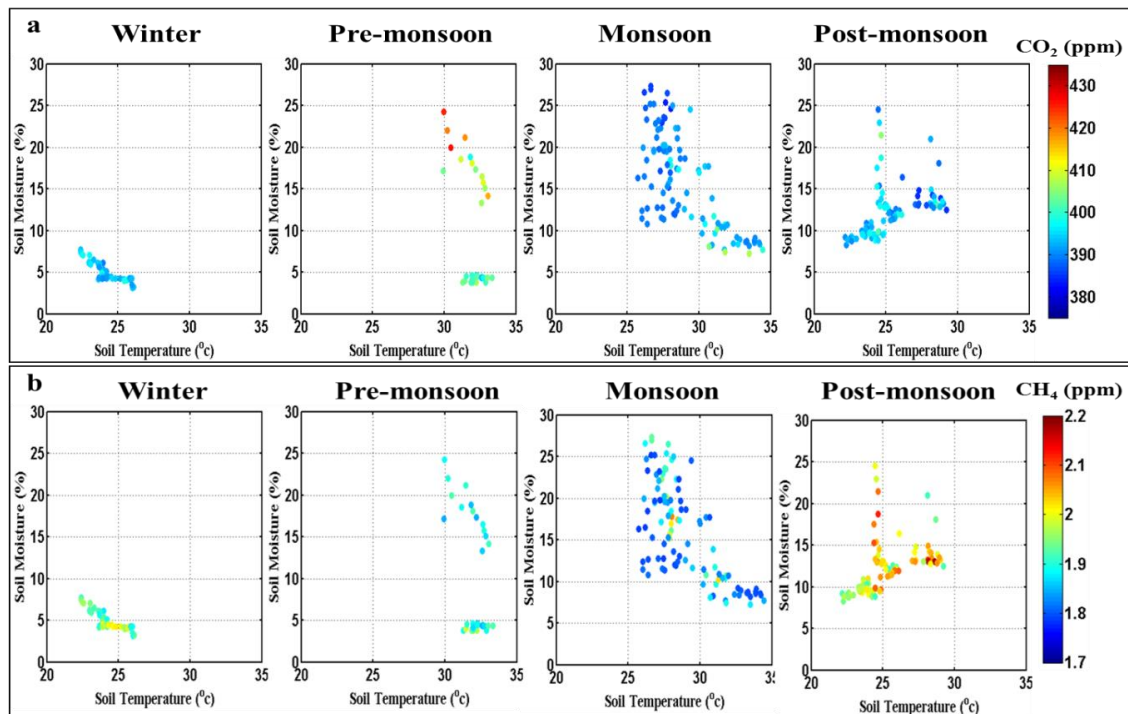
867 **Figure 5** a-d) Seasonal variations of diurnal averaged CO₂/CH₄ against boundary layer height
 868 during 2014



869 **Figure 6** a-b) daily mean scatterplot between wind speed and GHGs (CO₂ and CH₄).



873 **Figure 7** a-b) Daily means seasonal variation of CO₂ and CH₄ as function of humidity and air
 874 temperature during 2014



875 **Figure 8** a-b) Daily means seasonal variation of CO₂ and CH₄ as function of soil temperature
 876 and soil moisture during 2014

877

878

879

880

881

882

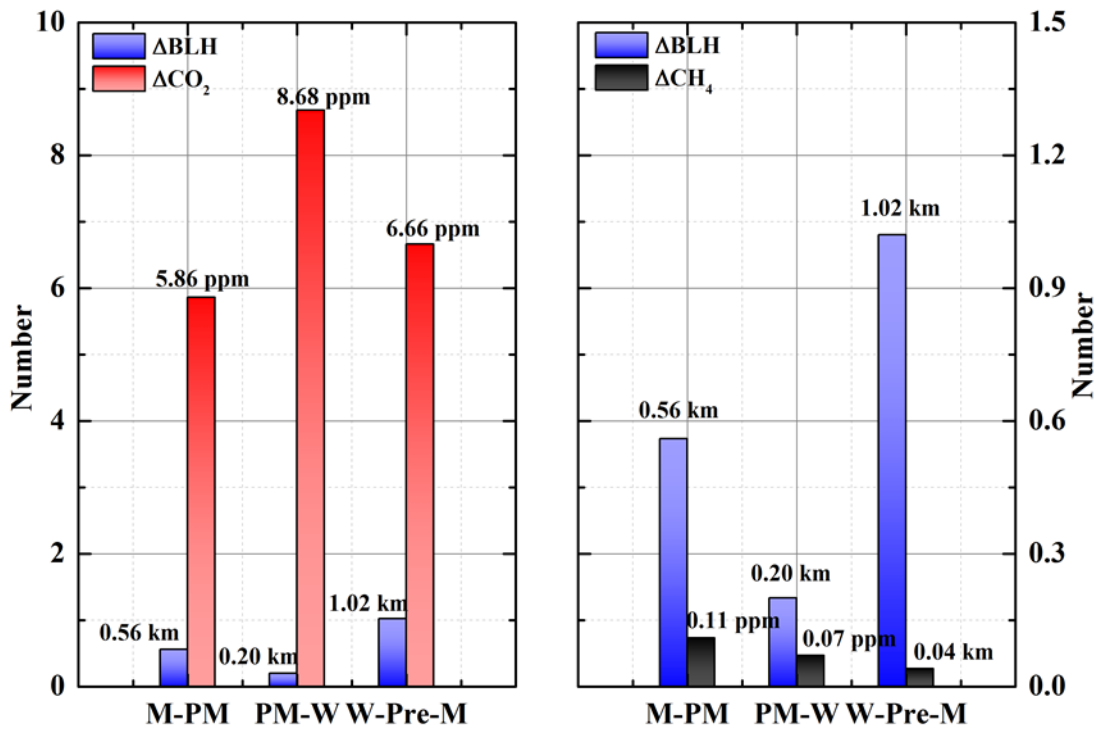
883

884

885

886

887



888 **Figure 9** seasonal differences in BLH against respective change in a) CO₂ and b) CH₄

889

890

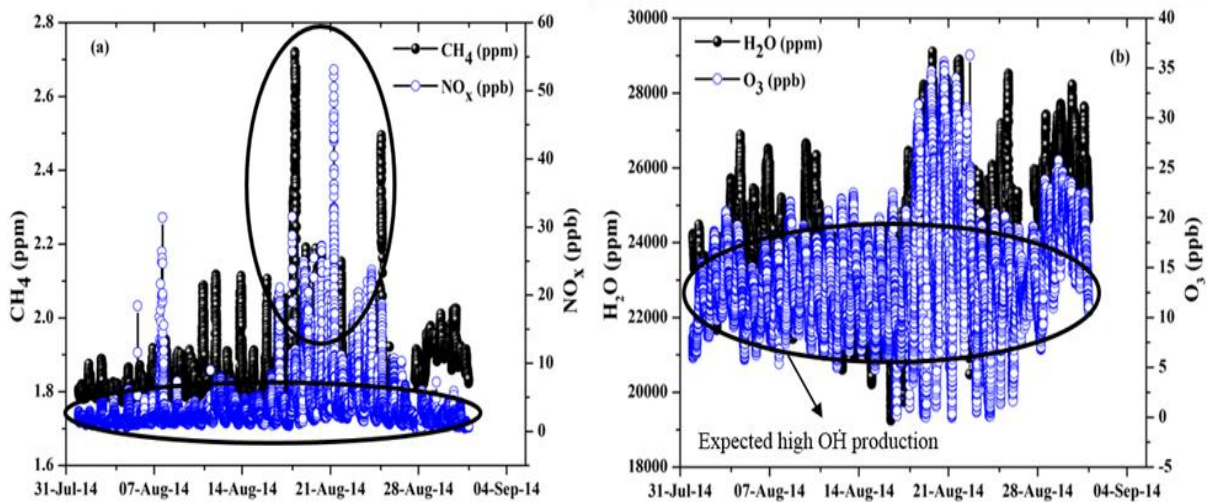
891

892

893

894

895



896

897 **Figure 10** Time series analysis of a) CH₄ vs. NO_x, b) H₂O vs. O₃

898

899

900

901

902

903

904

905

906

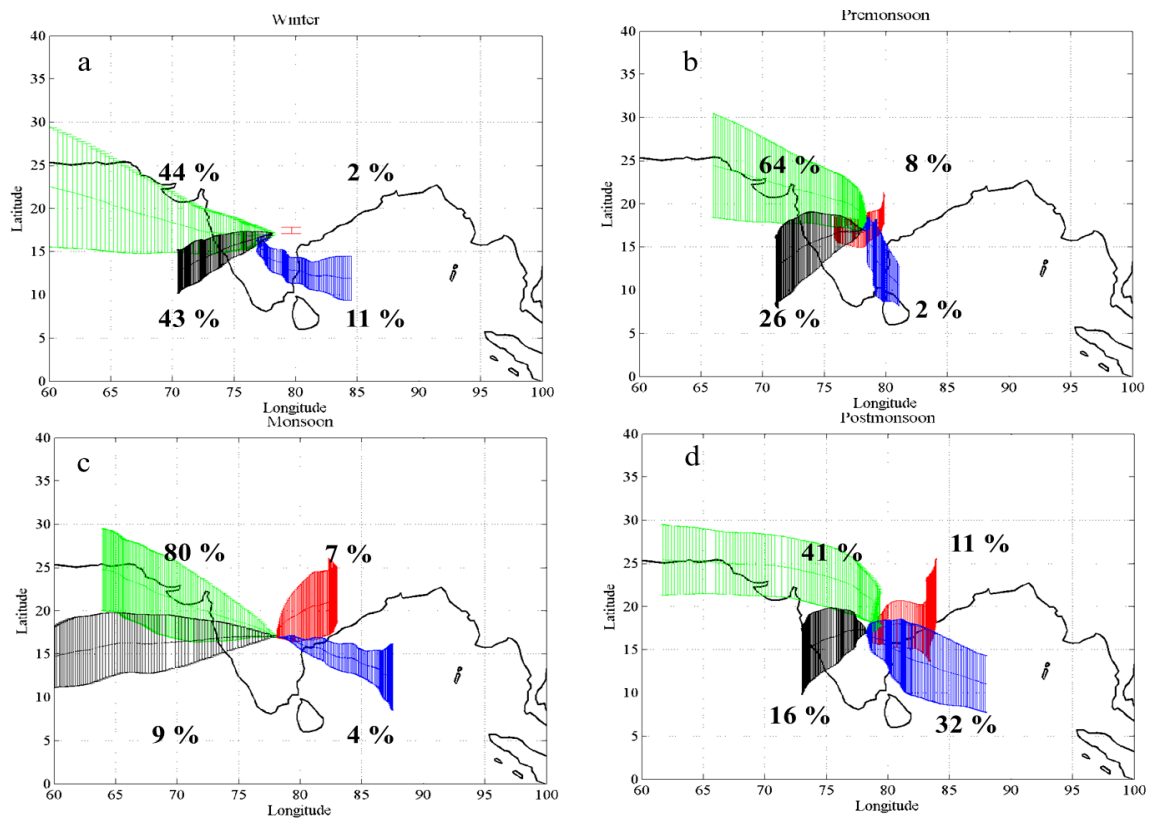
907

908

909

910

911



912 **Figure 11** a-d) Long range circulation of air mass trajectories ending over Shadnagar at 3 km

913 during winter, pre-monsoon, monsoon and post-monsoon.

914